Geomechanical Modeling of Reservoir Compaction, Surface Subsidence, and Casing Damage at the Belridge Diatomite Field

J. T. Fredrich, SPE, Sandia National Laboratories; **G. L. Deitrick**, Shell E&P Tech. Co.;
J. G. Argüello, Sandia National Laboratories; **E. P. DeRouffignac**, SPE, Shell Int. E&P Co.

Summary

Geologic, and historical well failure, production, and injection data were analyzed to guide development of three-dimensional geomechanical models of the Belridge diatomite field, California. The central premise of the numerical simulations is that spatial gradients in pore pressure induced by production and injection in a low permeability reservoir may perturb the local stresses and cause subsurface deformation sufficient to result in well failure. Time-dependent reservoir pressure fields that were calculated from three-dimensional black oil reservoir simulations were coupled uni-directionally to three-dimensional non-linear finite element geomechanical simulations. The reservoir models included nearly 100,000 gridblocks (100-200 wells), and covered nearly 20 years of production and injection. The geomechanical models were meshed from structure maps and contained more than 300,000 nodal points. Shear strain localization along weak bedding planes that causes casing dog-legs in the field was accommodated in the model by contact surfaces located immediately above the reservoir and at two locations in the overburden. The geomechanical simulations are validated by comparison of the predicted surface subsidence with field measurements, and by comparison of predicted deformation with observed casing damage. Additionally, simulations performed for two independently developed areas at South Belridge, Sections 33 and 29, corroborate their different well failure histories. The simulations suggest the three types of casing damage observed, and show that although water injection has mitigated surface subsidence, it can, under some circumstances, increase the lateral gradients in effective stress, that in turn can accelerate subsurface horizontal motions. Geomechanical simulation is an important reservoir management tool that can be used to identify optimal operating policies to mitigate casing damage for existing field developments, and applied to incorporate the effect of well failure potential in economic analyses of alternative infilling and development options.

Introduction

Well casing damage induced by formation compaction has occurred in reservoirs in the North Sea, the Gulf of Mexico, California, South America, and Asia.[1-4] As production draws down reservoir pressure, the weight of the overlying formations is increasingly supported by the solid rock matrix that compacts in response to the increased stress. The diatomite reservoirs of Kern County, California are particularly susceptible to depletion-induced compaction because of the high porosity (45-70%) and resulting high compressibility of the reservoir rock. At the Belridge Diatomite field, located ~45 miles west of Bakersfield, California, nearly 1000 wells have experienced severe casing damage during the past ~20 years of increased production.

The thickness (more than 1000 feet), high porosity, and moderate oil saturation of the diatomite reservoir translate into huge reserves. Approximately 2 billion bbl of original oil in place (OOIP) are contained in the diatomite reservoir and more than 1 billion bbl additional OOIP is estimated for the overlying Tulare Sands. The Tulare is produced using thermal methods and accounts for three-quarters of the more than 1 billion bbl produced to date at Belridge.[5] Production from the diatomite reservoir is hampered by the unusually low matrix permeability (typically ranging from 0.1 to several mDa), and became economical only with the introduction of hydraulic fracturing stimulation techniques in the 1970's.[6] However, increased production decreased reservoir pressure, accelerated surface subsidence, and increased the number of costly well failures in the 1980's. Waterflood programs were initiated in the late 1980's to combat the reduced well productivity, accelerated surface subsidence, and subsidence-induced well failure risks. Subsidence rates are now near zero; however, the well failure rate, although lower than that experienced in the 1980's, is still economically significant at 2-6% of active wells per year.

In 1994 a cooperative research program was undertaken to improve understanding of the geomechanical processes causing well casing damage during production from weak, compactable formations. A comprehensive data base, consisting of historical well failure, production, injection, and subsidence data was compiled to provide a unique, complete picture of the reservoir and overburden behavior.[7,8] Analyses of the field-wide data base indicated that two-dimensional approximations[9-11] could not capture the locally complex production, injection, and subsidence patterns, and motivated large-scale, three-dimensional geomechanical simulations. Intermediary results for Section 33 that used preliminary reservoir flow and material models were reported earlier.[8] This paper presents results for best-and-final simulations that used improved reservoir flow models, more sophisticated material models, and activated contact surfaces. The simulations were performed for two independently developed areas at South Belridge, Sections 33 and 29.

Reservoir Geology

The Belridge field is developed on two elongated northwestward-trending anticlines (**Fig. 1**) that are structurally offset by the Middle Belridge fault.[12-14] In this paper, the term

This paper (SPE XXXXX) was revised for publication from paper SPE 47284, prepared for presentation at the SPE/ISRM Eurock '98 held in Trondheim, Norway, 8–10 July 1998. Original manuscript received for review XX XXX 1999. Revised manuscript received XX April 2000. Paper peer approved XX XX 2000.

DISCLAIMER

DISCLAIMER

Portions of this document may be illegible in electronic image products. Images are produced from the best available original document.

Belridge field is used collectively to include development on both the northern (North Belridge) and southern (South Belridge) anticlines. The field contains two hydrocarbon reservoirs that are produced independently of one another: the diatomite (as used here, this includes both diatomite and porcelanite lithologies), and the overlying Tulare.

The diatomite reservoir produces 10-34° gravity oil from depths of about 800 to 3000 feet, depending upon structural position. The diatomite is a biogenic siliceous deposit consisting of the shells or tests of diatoms with varying amounts of detrital material (principally clay and sand) so that individual depositional cycles are identifiable, with the rock ranging from fairly pure to shaley diatomite. In the upper reservoir intervals, diatoms are preserved as opal-A, which is an amorphous, colloidal form of silica. Porosity ranges from 50-70%. With increasing depth (pressure) and temperature, the dominant mineralogic phase changes from opal-A to opal-CT. The associated reduction in porosity (<45%) makes the diatomite reservoir significantly less productive below the opal-CT transition. Below this, the diatom skeletal structures are no longer well preserved and the rock is a porcelanite.

The diatomite is unconformably overlain by the Plio-Pleistocene-aged Tulare Formation on the crest and by the Pliocene-aged Etchegoin and San Joaquin Formations on the flanks (Fig. 1). The Tulare is the second reservoir at Belridge and produces 11-14° gravity oil from multiple, highly discontinuous reservoir sands totaling about 400-1500 feet in thickness.[15] The sands were deposited in a prograding fluviodeltaic depositional setting and exhibit distinct lithofacies. Mudstones are present as laterally continuous, discrete beds (tens of feet thickness) separating the major sand intervals as well as at the interface between the Tulare and Belridge Diatomite. Mudstones are also present as thin beds (inches in thickness) within individual sands. Overlying the Tulare is 100-200 feet of unsaturated alluvium (Fig. 1).

Production, Injection, Subsidence, and Well Failures

Four independent operators currently produce the Belridge diatomite: Aera Energy LLC, Crutcher-Tufts Prod. Co., Exxon Co. USA, and Texaco Inc. Aera Energy, Texaco, and Exxon also produce the overlying Tulare from separate wells using steam flooding and cyclic steaming.

Development History. The diatomite reservoir received renewed attention in the 1970's with the introduction of hydraulic fracturing technology.[6] However, increased production resulted in significant reservoir compaction. By 1987, 10-15 feet of cumulative surface subsidence was estimated in some portions of the field and more than 100 wells were being abandoned annually due to severe casing damage. Waterflood programs were initiated in the late 1980's to mitigate subsidence, to reduce the potential for additional well failures, and for secondary recovery.

The low permeability of the diatomite has led to tight development with typical well spacings of 2½-acre (330 feet) to ⅝-acre (82.5 feet). Multiple hydraulic fracture treatments are conducted in production and injection wells with typical fracture heights and lengths (tip-to-tip) of 100-300 and 200-300 feet, respectively. Production wells are usually completed in both the diatomite and upper porcelanite intervals. The four operators are conducting pressure maintenance programs, with the exception of Aera Energy's leases in Middle and North Belridge that are still on 2½-acre primary development.

Mechanisms for Well Failure. Various mechanisms for casing damage are recognized, including compression, tension, and shear.[1-3,9,10] Compressional failures can occur within the producing interval due to large vertical strains associated with compaction. Tensile failures can result when material outside of the compacting zone provides vertical support to material above the compacting zone (arching). Thermal expansion due to steam injection in the Tulare may also contribute to development of tensile stresses in the overburden at Belridge.[9] Shear failures can be induced by horizontal displacements along the flanks of a subsidence bowl or by localized slip along weak bedding planes or reactivated faults in the overburden above the reservoir.

At Belridge, compressional failures at depths as great as 1800 feet have been observed. However, field observations of casing deformations in the overburden suggest a dominant shear mechanism. Several tensile failures at casing connectors in the overburden were also observed in the 1980's.

Field-Wide Database. To examine the statistical distribution of well failures in space and time at the Belrdige field, a comprehensive database was assembled that is described in detail elsewhere.[7,8] The database includes production (oil, water, and gas) and injection data from more than 3500 wells for 1984-94, with more than 850 of those wells damaged severely enough to render the well incapable of producing or injecting fluids.

Field-wide net voidage (produced minus injected fluids) reached a peak in 1986-87; however, the field-wide peak in well failures occurred somewhat later in 1987-89.[7,8] A major concern is that although pressure maintenance programs have been in place in heavily developed areas since the late 1980's, a costly well failure rate of 2-6% of active wells per year has been sustained since ~1992 even though subsidence has been largely arrested. More than 90% of confirmed casing damage to date has been above the diatomite reservoir and is focused at two particular intervals: at the interface between the Diatomite and overlying Tulare Formation and at a second horizon 300-400 feet above the diatomite reservoir.[7,8] The well failures are not distributed uniformly in space on the field-scale but are distributed uniformly on the local scale. That is, in regions that experienced significant subsidence, well failures occur throughout the produced area rather than just along the perimeter or in the center of the subsiding region.[7-10]

Three-Dimensional Numerical Simulations

Detailed geomechanical models of South Belridge, Sections 33 and 29 were formulated to evaluate potential well failure mechanisms. In particular, analyses of the comprehensive database[7,8] revealed the following: (1) Well failures have not been eliminated by the pressure maintenance programs but have continued at an economically significant rate. Current well failure rates in some parts of the field are close to rates experienced prior to the waterflood. (2) The spatial distribution of well failures with respect to observed surface subsidence suggests that well damage is influenced by local

production and injection patterns. This is consistent with the observation that a number of wells have failed within 6 mo. to 1 yr. of operation. (3) Damage is concentrated at the interface between the diatomite reservoir and overburden and at a second interface in the overburden. (4) Field observations of sheared wells indicate that lateral offsets of up to a foot can occur over very short vertical distances (~ten feet).

These observations motivated development of a model to examine the role of local gradients in effective stress in inducing well casing damage.[9,10] The gradients in effective stress result from large gradients in pore pressure induced by aggressive production and injection in a low permeability reservoir (well spacings ranging from 2½ to ⅝ acre). Three-dimensional reservoir flow simulations were performed to calculate the time-dependent reservoir pressure field that was then input into three-dimensional nonlinear finite element geomechanical models. South Belridge, Section 33 was selected initially since this region of the field had been the focus of previous two-dimensional finite element studies.[9,10] Therefore rock mechanics data necessary to derive material models for the overburden and reservoir rock as well as the initial stress state were available. As a key validation for the modeling approach, additional simulations were performed for Section 29, which was developed independently of Section 33 and consequently has a markedly different well failure history.

Reservoir Flow Models. The reservoir fluid flow simulations cover virtually the entire north-south extent of the development in Sections 33 and 29. The Section 33 flow simulation spans an area 2078 feet by 3409 feet that includes 197 production and injection wells and covers 18 years of production history from 1978-95. Field data indicate that nearly a hundred of the wells in the model area have experienced major casing damage. The Section 29 model covers an area 2066 feet by 3090 feet, includes 85 production and injection wells, and comprises 19 years of production history from 1978-96. In contrast to Section 33, field data indicate that only about a dozen wells have had major casing damage.

Thirteen depositional cycles are identifiable within the diatomite reservoir, and transitions within many of these cycles divide them further into subcycles. Subcycles that pinch out as the crest is approached are grouped with the topmost cycle that does not, resulting in a 28 layer reservoir description. Structure, porosity, and initial oil saturation inferred from well logs were mapped by layer, and oil gravity measured from sidewall core samples was generally mapped by cycle. For the Section 33 model, the 28 layers were lumped to 9 layers (mostly by cycle), and the resulting property maps were interpolated to define the structure, porosity, oil saturation, and oil gravity for the reservoir simulation. For the Section 29 model, the G cycle was divided into two sub-cycles, resulting in a total of 10 layers. Initial gas saturation was set uniformly to 5%. Permeability was defined by permeability-porosity correlations determined from experimental measurements on core samples. Relative permeabilities (oil/water and gas/oil) were derived from previous two-dimensional reservoir simulations that were history matched to different portions of the field and were varied layer-by-layer according to each layer's maximum initial oil saturation.

The areal grids were 149×69 (yielding 92,529) gridblocks for the Section 33 model, and 126×66 (yielding 83,169) gridblocks for the Section 29 model, and meshed directly from geologic structure maps. The three-dimensional fluid flow calculation was performed using the black oil version of MORE® (Roxar ASA). Oil gravity variations were modeled using temperature-dependent PVT tables spanning a narrow temperature range. Wells with hydraulic fractures assumed to be uniformly oriented N11E[9] (parallel to the model boundaries) and with a tip-to-tip length of 250 feet were modeled by completing the well in each gridblock intersected by the fracture. Quarterly liquid production/injection rate constraints were set according to each well's production history. Producing and injecting bottomhole pressure constraints were 50 and 800 psi, respectively. Matching individual well performance, including water/oil ratio, was deemed important to obtain sufficiently accurate pressure fields, and the historical simulations compare well with the field performance (**Fig. 2**).

Geomechanical Models. To examine the influence of the production- and injection-induced pressure changes, the pore pressures calculated from the three-dimensional reservoir simulations were used as loads in three-dimensional nonlinear finite element geomechanical simulations. The geomechanical simulations were performed using Sandia's three-dimensional large-deformation quasi-static structural mechanics code JAS3D. The code is a hybrid of the Sandia codes SANTOS[16] and JAC[17], and employs iterative (explicit) solution procedures to achieve a high degree of computational efficiency that therefore enables the analysis of extremely large and complex models.

Structure. The finite element models were meshed directly from geologic structure maps of Sections 33 and 29, and defined such that the reservoir flow model forms a subset of the geomechanical model. There was a 1:1 correspondence between the reservoir flow and geomechanics models so that the time-dependent pressures defined for each of the gridblocks in the reservoir simulation were mapped uniquely to the appropriate elements in the finite element simulation. The mesh was then extended vertically to incorporate the overburden and underlying strata, and laterally to include areas outside of the field development as described below (**Fig. 3**).

The Section 33 and 29 geomechanical models are ~2100 feet wide × 13,100 feet long × 4500 feet deep, and ~2100 feet wide × 12,400 feet long × 4500 feet deep, respectively. The east-west extent of the geomechanical model (2100 feet) corresponds exactly to the east-west extent of the reservoir flow model. The development to the east and west of the flow model boundaries is similar to that within the model area whereas there is no development to the north and south. Thus, to remove boundary effects, the geomechanical model was extended by a factor of 2 along both the northern and southern boundaries in comparison to the fluid flow model. Addition of the extra blocks of material on the northern and southern ends of the reservoir flow model allows the material oustide the reservoir to deform in response to pressure depletion. Thus,

the areal extent of the geomechanical model is 3× the areal extent of the reservoir (Fig. 3). The geologic structure for the terminal portions of these northern and southern extents was extrapolated from structure maps.

As noted earlier, the reservoir, which includes both diatomite and porcelanite lithologies, is discretized into nine layers (ten for the Section 29 model) with a total thickness of about 1600 feet. Underlying the reservoir is the Lower Porcelanite, which is about 2200 feet thick with a vertical discretization of six elements. A more refined discretization is required for the overburden since the field data indicate that most confirmed casing damage occurs above the reservoir. Thus, the overburden, which totals about 650 feet in thickness, is more finely meshed with three stratigraphic layers and a total vertical discretization of ten elements. The three layers correspond to the Upper and Lower Tulare and the Air Sands (alluvium). The geomechanical models include three contact surfaces (see Fig. 3), which are discrete surfaces along which discontinuous displacements can occur. The contact surfaces are numerical analogues for thin mudstones that field data suggest are preferred sites for shear casing damage. One contact surface is located immediately above the reservoir and corresponds to a prominent claystone identified in well logs that unconformably overlies the Belridge Diatomite. Two additional contact surfaces are located at distinct stratigraphic horizons in the overburden.

The Section 33 geomechanical model contains 391,500 nodal points with 331,525 eight-node Lagrangian uniform-strain elements, whereas the Section 29 model contains 325,080 nodes and 276,250 elements.

Material Models. The overburden formations, consisting of the Upper and Lower Tulare and Air Sands, are described using Drucker-Prager constitutive models.[8-10] The lowermost layer of the diatomite reservoir and the underlying Porcelanite are described similarly. The upper eight layers (nine for the Section 29 model) of the reservoir are modeled using a cap plasticity model which includes both a shear failure surface and a second yield surface (cap) to account for inelastic compaction at stress states below the failure surface. The Sandia cap model is a generalized version of the Sandler and Rubin cap plasticity model.[20] Each layer of the geomechanical model (Fig. 3) is associated with a specific material model, so that within any single layer, the same material model is applied within the reservoir area as in the extended (flank) regions of the model. Constitutive parameters are given in **Tables 1** and **2**, and Refs. 18 and 19 describe the cap plasticity model and a method for parameter estimation using laboratory rock mechanics triaxial compression test data.

Contact Surfaces. As noted, the contact surfaces are intended to model the behavior of thin shales located above the reservoir and in the overburden. Because the friction coefficients along the contact surfaces are the only free parameters in the geomechanical simulations, multiple simulations were performed with the Section 33 model that used different parameter values. One simulation was performed with the contact surfaces fixed. A second was performed with a uniform friction coefficient of 0.2. A third was performed with friction coefficient varied as follows: 0.05 on the uppermost contact surface, 0.105 on the intermediate contact surface, and 0.11 on the contact surface located at the interface between the diatomite reservoir and overburden. The parameter values for the third simulation were based on analyses of a two-dimensional cross-sectional model that varied friction coefficients in an attempt to match qualitatively the observed distribution of casing damage with depth (see previous discussion). The two-dimensional model was a single slice of the three-dimensional Section 33 model, and the slice was selected at random from the central area. No further attempts at history matching were performed for the three-dimensional geomechanical models. The results shown for the Section 33 model are for this latter simulation with varied friction coefficients, and the Section 29 simulation used these same values.

Boundary Conditions and Initial (Tectonic) Stresses. The four vertical faces of the geomechanical model (see Fig. 3) were free to displace vertically and in directions parallel to the boundary, but constrained from displacing in the direction perpendicular to the boundary. The bottom of the model was fixed whereas the top (i.e., earth surface) was free to displace in all directions. The prescribed initial tectonic stress state prior to reservoir depletion has a significant impact on the numerical results because of the non-linearity of the material models. The initial stress state at time zero was prescribed following Hansen et al.[9] The vertical (total) principal stress due to gravitational loading was calculated directly on an element by element basis from the bulk density of the overlying materials with initial pore pressures in the different stratigraphic layers calculated as described in Ref. 9. The two effective horizontal principal stresses, that are initially oriented parallel to the model boundaries, were calculated for each element by multiplying the effective vertical stress previously computed by factors of 0.65 and 1.20.[9]

The model's response to the application of the *in situ* stresses (referred to as the geostatic step) serves as a quality check. Large inelastic deformations and/or the appearance of shear components in the stress tensor may indicate that the imposed initial stress state is not consistent with the geomechanical model. (Note that the principal stress directions are not constrained to remain parallel to the model boundaries.) The maximum vertical surface displacement following the geostatic step was a few inches, and this was considered adequate given the total model thickness of several thousand feet. Following application of the *in situ* stresses and the model's equilibration (or relaxation) to this imposed initial stress state, the displacements are zeroed, and the (elemental) stress state that the model relaxes to served as the input (elemental) stress state for the first time step of the simulation. The imposed gravity and tectonic loads are active during the entire simulation.

Simulation Results. The databases for the geomechanical simulations consist of the nodal displacements and the elemental stress tensors as a function of time. Three aspects of the simulations are of particular interest: vertical compaction at the top of the model (surface subsidence); nodal displacements along vertical trajectories (well deformations); and evolution of the *in situ* stress field. (Principal stresses evolve with production and injection, an effect that has important implications for hydraulic fracture re-orientation during infill drilling). Results for only the first two analyses

are presented here.

Surface Subsidence. The simulations predict well the overall location, shape and approximate amount of surface subsidence with time. Quantitative comparison of predicted versus measured cumulative surface subsidence is complicated by the very sparse monument survey coverage that existed prior to the 1990's, and also by uncertainties in the baseline survey data. To negate difficulties associated with the latter, predicted versus measured subsidence rates (in inches) are shown in **Fig. 4** for the Section 33 simulation and in **Fig. 5** for the Section 29 simulation. In both simulations, a primary bowl aligned with the trend of the structure starts to form over the reservoir in the early 1980's. Predicted maximum cumulative subsidence over the Section 33 model area is ~3 feet by 1985, ~5½ feet by 1989, ~6½ feet by 1992, and ~7 feet by 1995 (the end of the simulation). Corresponding maximum cumulative subsidence over the Section 29 model area is ~1½ feet by 1985, ~3½ feet by 1989, ~4 feet by 1992, and ~5 feet by 1995.

In the Section 33 simulation (Fig. 4), the substantial subsidence rates (several in/yr) predicted during the early-to-mid 1980's correspond to 2½-acre primary production. Higher rates of subsidence (5-10 in/yr) predicted during the late 1980's are a consequence of a 1986-90 peak in production due to a 1¼-acre infilling program conducted during 1986-87. Subsidence rates reach a peak in 1987 when a rate of 10 in/yr is predicted over much of the model area (Fig. 4, upper left). The section-wide waterflood initiated in 1987 causes a rapid decline in subsidence rates to 5 in/yr or less, with small amounts of rebound predicted in the upper right region of the model (Fig. 4, upper right). Increased production in the southeastern part of Section 33 during that time causes the formation of a secondary bowl in ~1987 which persists through the end of the simulation and is corroborated by the field monument data. The reduced subsidence rates predicted in the 1990's (generally less than 5 in/yr, with some areas showing uplift of 1-3 in/yr) reflect the maturity of the waterflood and the declining production (as compared to the late 1980's). 1990 is the first year for which monument survey data are available, and the predicted subsidence rates over the last seven years of the simulation show reasonable agreement with the survey data, typically to within a couple to few inches (Fig. 4, bottom). In general, overall trends are matched.

As discussed above, predicted subsidence rates for the Section 29 simulation (Fig. 5) are reduced in comparison to the Section 33 simulation (Fig. 4), which results from the lower productivity of Section 29 versus Section 33 (Fig. 2). Although a section-wide water injection program was not initiated in Section 29 until 1990 (as compared to 1987 for Section 33), Section 29 was produced less aggressively than Section 33. Modest subsidence rates of up to 2 in/yr are predicted during the early 1980s. Predicted rates increase from 1985 through 1989 in response to increased production resulting from newly drilled wells (see Fig. 2). A more pronounced subsidence bowl that appears initially on the eastern half of the model area in 1985 (Fig. 5, upper left) spreads and uniformly covers the central area of the model by 1989 (Fig. 5, upper right). 1989 is the first year that monument survey data exist, and the single data point indicating a rate of 6 in/yr agrees very well with the model prediction. In 1989 a 1¼-acre infilling program was initiated, and during the first year, infill wells were produced before older producers were converted to injection. Thereafter, predicted subsidence rates decrease through the early 1990s in response to the water injection program, and the model predictions agree reasonably well with the monument survey data (Fig. 5, bottom).

As compared to the Section 33 simulation, the cumulative and incremental subsidence rates are both smaller in magnitude and more uniform over the model area. This is consistent with both the more regular development and the more uniform operating policies (production and injection rates) that were applied across Section 29 as compared to Section 33 which was the site of several pilots (see Fig. 2).

Well Casing Damage. Shear deformations are maximized along the contact surfaces. **Fig. 6** shows the predicted shear displacement parallel to the hydraulic fracture direction (the *y*-direction) at a contact surface over a single 1-yr period (1990-91) for the Section 33 and 29 simulations. The *y*-direction corresponds to the long dimension of the model, and is thus roughly perpendicular to the contours of the subsidence bowl (or more properly, trough) that traverses the field. The model predictions shown are for the contact surface that corresponds to the top of the diatomite reservoir, as this is the horizon at which most confirmed casing damage is concentrated. The time step shown is representative of the 5-year period from 1987 through 1991 over which the simulations for the Section 33 model predict severe shearing displacements of ±½ ft/yr over extensive regions within the section. The initial occurrence of a shearing deformation of ½ ft/yr occurs in 1984 at the precise location of a small waterflood pilot (consisting of 4 injectors) that was initiated in the southeastern portion of the Section 33 model area in 1983. A second nucleus appears in 1986 that is located at the northwestern edge of the field development along what is essentially the flank of the subsidence bowl. Although limited in extent, these regions of predicted intense shear deformation expand in lateral extent through the start of 1987, which marks the year in which the waterflood was expanded to the rest of Section 33. The aggressive initiation of a section-wide waterflood has an immediate and dramatic impact on the predicted shear deformation, with displacements of ±½ ft/yr predicted over large areal extents through the end of 1990 (see Fig. 6, left). In 1990, the water injection rates were reduced substantially (see Fig. 2), and the effect on shearing displacement is again dramatic, with the areal extent of severe shearing displacement reduced substantially for time steps following the start of 1991. While small regions with predicted displacements of ±½ ft/yr persist thoughout the rest of the simulation, these regions are very limited in their lateral extent.

The shear displacement field at the top of the diatomite in the *x*-direction (perpendicular to hydraulic fractures and parallel to the short dimension of the model) is qualitatively similar to that in the *y*-direction. However, the magnitudes are reduced, and the regions exhibiting the maximum predicted displacement of ±½ ft/yr are limited in areal extent. While the predicted shearing displacements at the two contact surfaces located higher up in the overburden show similar trends, the magnitudes are in general markedly reduced in comparison to those observed at the contact surface located immediately above the reservoir.

The model predictions for Section 29 differ dramatically. Whereas large portions of the Section 33 model area undergo incremental shear displacements of ½ ft/yr over repeated successive years, predicted shear deformations for the Section 29 simulation reach ½ ft/yr only in a very small number of instances with extremely restricted lateral extent. Comparison of the results for Sections 33 and 29 (Fig. 6) provides a direct global measurement of their relative proclivity for well casing damage. The results corroborate uneqivocally the vastly different well failure histories observed for the two sections.

The x, y, and z displacement fields along vertically-oriented lines that coincide with well locations can be equated to casing deformations. Both the timing and magnitude of the predicted and observed deformation were compared systematically for the Section 33 simulation, with good agreement for the majority of the nearly 200 wells. An example of predicted deformation for an arbitrarily selected well is shown in **Fig. 7**. The left plot shows the horizontal x-displacement (perpendicular to the hydraulic fracture orientation) as a function of depth. The temporal and vertical character of the displacement field contains several important features. First, the large change in mechanical properties at the interface between the diatomite reservoir and Lower Tulare coupled with the sliding contact surface introduces a major discontinuity in the horizontal displacement field with depth. Second, the predicted x-displacements are small until 10.0 yrs, which is just prior to the onset of the waterflood and conversion of this particular well to injection. This well's conversion from production to injection coincides exactly with the development of severe shearing displacements at the well location. This illustrates precisely the finding discussed earlier; namely, that the waterflood that was implemented in part to reduce the well failure risk, in many cases amplified the horizontal shearing displacements that were experienced by wells. Displacement in the horizontal y-direction (middle plot) is substantially larger than that in the x-direction, and this largely reflects the formation of a subsidence bowl as material flows inwards in response to pressure depletion. The right plot shows vertical z-displacements. Particularly significant is that the maximum z-displacement occurs at the top of the diatomite reservoir, rather than at the surface. Thus, differential compaction caused by production from the underlying reservoir puts the overburden in a state of relative tension. This result is consistent with field observations of tensile failures of relatively weak casing connectors used in earlier wells. Finally, large z-displacements that occur at depth in the reservoir (~2 feet of relative offset) imply a strong possibility for compressional damage, which agrees with field observations.

An important result of the well analyses for the Section 33 model relates to the lack of uniformity in the predicted well deformations. That is, the wells show remarkable individuality in their response to production and injection. This reflects precisely the highly localized nature of the spatially and temporally varying pore pressure field (and thus effective stress) that surrounds wells, the influence of nearby producers and injectors on well response, and the central role of the local stress changes in driving casing damage at the Belridge field.

Effects of Cap Plasticity and Contact Surface Friction. Two aspects of the numerical simulations warrant further mention. First, the use of a cap plasticity model for the diatomite formation has substantial impact on the numerical results. The cap plasticity model is a multiple surface constitutive model that includes a second yield surface that accounts for inelastic compaction at stress states below the shear failure surface.[18,19] Use of this type of model thus increases substantially the run time of the simulation. Two earlier simulations[8] that were performed with the Section 33 model (using a slightly different reservoir flow simulation as input) applied a Drucker-Prager rather than a cap plasticity model for the reservoir formation. Those results showed that use of the cap plasticity model increased predicted subsidence by up to a factor of 2. While it might be possible to obtain a similar magnitude with a Drucker–Prager (or Mohr Coulomb) model by reducing artificially the bulk and elastic moduli of the reservoir formation, such an approach would obviously not represent accurately the behavior of the compacting reservoir.

The second point relates to the friction coefficients at the contact surfaces that as described earlier were varied in different simulations for the Section 33 model. While the model results are sensitive to friction coefficient at the contact surfaces, similar qualitative behavior is obtained regardless of friction coefficient. A simulation that was performed with the Section 33 model with the contact surfaces fixed showed that even in the absense of a frictional contact, shear deformation was still focused at the horizon between the diatomite reservoir and overburden.[8] The significant mechanical contrast at the boundary between the compacting reservoir and stiffer overburden acts to focus shear deformations at that interface. The inherent focusing of shear deformation at the contact is further amplified with an activated contact surface. In this regard, also note that as described earlier, the friction coefficient on the contact surface that has the most severe shearing displacements (at the top of the reservoir) has the highest friction coefficients of the three contact surfaces in the model (0.11). While the predicted surface subsidence also exhibits some sensitivity to the friction coefficients, no attempts were made to history match the three-dimensional models with the monument survey subsidence data.

Discussion

Analyses of the field-wide database consisting of historical well failure, production, and injection data at Belridge suggested that casing damage is influenced strongly by local production and injection patterns. This observation motivated us to examine the role of local gradients in effective stress in inducing well casing damage. The gradients in effective stress result from large gradients in pore pressure induced by aggressive production and injection in a low permeability reservoir (well spacings ranging from 2½ to ⅝ acre). Our ultimate goal was to develop a predictive tool to enable improved reservoir management. The approach that we took to accomplish this consisted of developing three-dimensional geomechanical models of the Belridge field and implementing non-linear finite element numerical simulations to analyze the reservoir and overburden response during primary and secondary recovery.

Our work represents a significant advance over previous studies[3,4,9-11] in several regards. The numerical simulations reported here are at a dramatically larger scale than the

previous work[3,4,9-11] which was limited to two-dimensional finite element analyses. The models developed here are at the section scale and include hundreds of wells; furthermore, the models are three-dimensional, which as discussed earlier is central for elucidating the field observations of casing damage. Our effort also included[18] the systematic development of cap plasticity models to describe accurately the behavior of the compacting reservoir formation. Moreover, while the previous work has focused on the effect of prescribed uniform drawdowns on reservoir and overburden behavior, this work has applied one-way coupling between large-scale three-dimensional reservoir flow and geomechanical simulations. All of these features are key for the practical application of geomechanical simulation as a reservoir management tool.

The significant insight into the reservoir behavior gained through the one-way coupled modeling approach applied here also serves to further stimulate development of two-way[21] and fully coupled reservoir flow–geomechanics simulators. While either a two-way or fully coupled approach is highly desirable from a phyiscal point of view, the numerical issues are complex and require significant development for the reservoir-scale modeling of interest here.

Mitigation and Reservoir Management. This work demonstrates clearly both the utility and practicality of applying three dimensional geomechanical modeling to understand and predict behavior at both the well and reservoir scale during production. The modeling approach is validated by quantitative comparisons of predicted and observed surface subsidence for the Section 33 and 29 models, and by rigorous comparison of predicted and observed casing deformation for the Section 33 model (not discussed here). The Section 29 simulation provides additional and pivotal validation by corroborating the markedly different well failure history observed there. Thus, the geomechanical simulation approach has been established as a reservoir management tool to mitigate well failures and surface subsidence.

Geomechanical simulation can be applied in forecasting to identify optimal operating policies to mitigate casing damage for existing field developments, and also to incorporate the effect of well failure potential in economic analyses of alternative development options. For example, geomechanical simulations can be performed to assess quantitatively the effects of different producer to injector ratios, well density (spacing), relative timings of infill wells, and initiation or expansion of secondary recovery methods such as waterflooding on well failure potential and subsidence. For existing field developments, analyses can be conducted to optimize injection profiles, or to assess the impact of converting existing wells from producers to injectors. The operator has undertaken such analyses and found that incorporation of geomechanical modeling into reservoir management has had a significant impact on their identification of optimal development options.

Conclusions

1. Three-dimensional nonlinear finite element geomechanical simulations reveal the evolution of the subsurface stress and displacement fields in the reservoir and overburden, and show how local production and injection patterns affect their spatial and temporal variation. The simulations of Sections 33 and 29 successfully reproduce the approximate magnitude, location, and shape of the subsidence bowl, as well as details of its incremental growth. The simulations show that although water injection has mitigated surface subsidence, it can, under some circumstances, also increase the lateral gradients in effective stress that in turn can accelerate subsurface horizontal motions. At Belridge, the prediction of severe shearing deformations (± ½ ft/year) at the interface between the diatomite reservoir and overburden coincides with the initiation and progression of an aggressive water injection program. The predicted cessation of a several year period of severe shearing deformations corresponds to the introduction of more moderate injection rates.

2. The geomechanical simulations suggest three types of casing failure: shear failures above the reservoir and in the overburden, tensional failures in the overburden, and compressional failures in the reservoir. Shear failure results from discontinuities in the horizontal displacement field at weak bedding planes or at major mechanical interfaces and dominates observed casing damage. Compressional damage is predicted in the compacting reservoir where vertical compressional strains can be substantial. Differential compaction between the reservoir and overburden causes tensile stresses in the overburden that can result in well failure. The simulations performed for two independently developed areas at Belridge, Sections 33 and 29, predict the markedly different casing damage histories observed in the two sections. The simulations predict semi-quantitatively the timing, location, and depth of casing damage. The simulations corroborate the importance of the locally varying stresses in influencing casing damage potential.

4. The methodology and geomechanical simulation approach developed in this work is being applied as a reservoir management tool to mitigate surface subsidence and well failures. Geomechanical simulation is applied in forecasting to incorporate the effect of well failure potential in economic analyses of alternative development options, and to identify optimal operating policies to mitigate casing damage for existing field developments.

Nomenclature

A = shear failure surface material parameter, psi
B = shear failure surface material parameter, psi^{-1}
C = shear failure surface material parameter, psi
D_1 = cap hardening material parameter, psi^{-1}
D_2 = cap hardening material parameter, psi^{-2}
E = Young's modulus, psi
G = shear modulus, psi
K = bulk modulus, psi
R = ratio of principle ellipse radii of cap surface
W = cap material parameter, dimensionless
X_0 = initial cap position, psi
α = Ducker-Prager material parameter
κ = Drucker-Prager material parameter, psi
ν = Poisson's ratio, dimensionless
ρ = bulk density, $slugs/ft^3$

Acknowledgments

This work was supported by the U.S. Department of Energy's (DOE) Natural Gas and Oil Technology Partnership Program. Aera Energy LLC and the US DOE National Petroleum Technology Office provided additional funding. We thank T. A. Moroney and R. L. Gwinn of Aera for their significant technical contributions to this project. We are grateful to A. F. Fossum for implementing the cap constitutive model, and contributions of B. J. Thorne and D. S. Preece are also acknowledged. Tom Moroney provided Fig. 1. This work was performed as part of an ongoing collaborative project between Sandia, Lawrence Berkeley, and several industry partners. We have benefited in particular from discussions with Larry Myer, Mike Bruno, and Wolfgang Wawersik. An earlier version of the manuscript was improved by a careful review by Kirk Hansen, and we are also grateful to three anonymous reviewers for their helpful suggestions. This work was performed at Sandia National Laboratories funded by the U.S. DOE under Contract No. DE-AC04-AL85000. Sandia is a multiprogram laboratory operated by Sandia Corporation, a Lockheed Martin Company, for the U.S. DOE.

References

1. Yudovich, A. and Morgan, D. R.: "Casing Deformation in Ekofisk," *JPT* (July 1989) 729.
2. Bruno, M. S.: "Subsidence-Induced Well Failure," paper SPE 20058 presented at the 60th California Regional Meeting, Ventura, 4-6 April 1990.
3. Hamilton, J. M., Maller, A. V., and Prins, M. D.: "Subsidence-Induced Shear Failures Above Oil and Gas Reservoirs," *Proc. 33rd US Symp. on Rock Mechanics*, AA Balkema, Rotterdam (1992) 273.
4. Bruno, M. S. and Bovberg, C. A.: "Reservoir Compaction and Surface Subsidence Above the Lost Hills Field, California," *Proc. 33rd US Symp. on Rock Mechanics*, AA Balkema, Rotterdam (1992) 263.
5. "South Belridge 15th Billion Barrel Oil Field in US," *Oil and Gas J.* (15 Oct. 1995) 119.
6. Strubhar, M. K., Medlin, W. L., Nabi, S. M., and Andreani, F. S.: "Fracturing Results in Diatomaceous Earth Formations, South Belridge Field, California," *JPT* (March 1984) 495.
7. Myer, L., Jacobsen,, J., Horsman, J., Fredrich, J. T., Wawersik, W. R., Arguello, J. G., Bruno, M. S., and Qian, H.: "Use of Visualization Techniques in Analysis of Well Failures in Diatomite Reservoirs," *The Leading Edge* (March 1996) 185.
8. Fredrich, J. T., Arguello, J. G., Thorne, B. J., Wawersik, W. R., Deitrick, G. L., de Rouffignac, E. P., Myer, L. R., and Bruno, M. S.: "Three-Dimensional Geomechanical Simulation of Reservoir Compaction and Implications for Well Failures in the Belridge Diatomite," paper SPE 36698 presented at the 1996 SPE ATCE, Denver, 6-9 October.
9. Hansen, K. S., Prats, M., and Chan, C. K.: "Modeling Reservoir Compaction and Surface Subsidence at South Belridge," SPEPF (Aug. 1995), 134.
10. de Rouffignac, E. P., Karanikas, J. M., Bondor, P. L., and Hara, S. K.: "Subsidence and Well Failure in the South Belridge Diatomite Field," paper SPE 29626 presented at the 1995 SPE Western Regional Meeting, Bakersfield, 8-10 March.
11. Hilbert, L. B., Fredrich, J. T., Bruno, M. S., Deitrick, G. L., and de Rouffignac, E. P.: "2D Nonlinear Finite Element Analysis of Well Damage due to Reservoir Compaction, Well-to-Well Interactions, and Localization on Weak Layers," *Proc. 2nd No. Amer. Rock Mech. Symp.*, AA Balkema, Rotterdam (1996).
12. Graham, S. A. and Williams, L. A.: "Tectonic, Depositional, and Diagenetic History of Monterey Formation (Miocene), Central San Joaquin Basin, California," *AAPG Bull.* (1985) 69, No. 3, 385.
13. Schwartz, D. E.: "Characterizing the Lithology, Petrophysical Properties, and Depositional Setting of the Belridge Diatomite, South Belridge Field, Kern County, California," *Studies of the Geology of the San Joaquin Basin,* Graham (ed.), Pacific Section SEPM (1988), **60,** 281.
14. Bowersox, J. R.: "Geology of the Belridge Diatomite, Northern South Belridge Field, Kern County, California," *Structure, Stratigraphy and Hydrocarbon Occurrences of the San Joaquin Basin, California,* Kuespert and Reid (eds.) Pacific Sections of SEPM and AAPG (1990) 215.
15. McPherson, J. G. and Miller, D. D.: "Depositional Settings and Reservoir Characteristics of the Plio-Pleistocene Tulare Formation, South Belridge Field, San Joaquin Valley," *Structure, Stratigraphy and Hydrocarbon Occurrences of the San Joaquin Basin, California,* Kuespert and Reid (eds.) Pacific Sections of SEPM and AAPG (1990) 205.
16. Stone, C. M.: "SANTOS–A 2D Finite Element Program for the Quasi-static, Large Deformation, Inelastic Response of Solids," SAND90-0543, Sandia National Laboratories, Albuquerque, New Mexico (1996).
17. Biffle, J. H.: "JAC3D–A 3D Finite Element Computer Program for the Nonlinear Quasi-static Response of Solids with the Conjugate Gradient Method," SAND87-1305, Sandia National Laboratories, Albuquerque, New Mexico (1993).
18. Fossum, A. F. and Fredrich, J. T.: "Estimation of Constitutive Parameters for the Sandia Cap Model for Cycles G, H, I, J, K, L, and M, South Belridge Diatomite Field," SAND98-1407, Sandia National Laboratories, Albuquerque, New Mexico (1998).
19. Fossum, A. F. and Fredrich, J. T.: "Constitutive Models for the Etchegoin Sands, Belridge Diatomite, and Overburden Formations at the Lost Hills Oil Field, California," SAND2000-0827, Sandia National Laboratories, Albuquerque, New Mexico (2000).
20. Sandler, I. S. and Rubin, D.: "An Algorithm and a Modular Subroutine for the Cap Model," *Int. J. Num. Anal. Meth. Geo.*, (1979) **3**, 173.
21. Minkoff, S. E., Stone, C. M., Arguello, J. G., Bryant, J., Peszynska, M., and Wheeler, M.: "Coupled Geomechanics and Flow Simulation for Time-Lapse Seismic Modeling," *Proc. 69th Ann. Int. Mtg. SEG* (1999), Houston, 1667.

SI Metric Conversion Factors

bbl × 1.589 873	E-01 = m^3
ft × 3.048*	E-01 = m
in × 2.54*	E+00 = cm
md × 9.869 233	E-04 = μm^2
psi × 6.894 757	E-03 = MPa
$slug/ft^3$ × 515.379	E+00 = kg/m^3

* Conversion factors are exact.

Joanne T. Fredrich is a Principal Member of Technical Staff in the Geophysical Technology Department at Sandia National Laboratories in Albuquerque, New Mexico. e-mail: fredrich@sandia.gov. Her interests include geomechanics, mechanical and physical properties of geomaterials, 3D imaging, and fluid flow in porous media. She holds a BS (Honors) degree in geology from the State University of New York, Stony Brook, and a PhD degree in geophysics from the Massachusetts Institute of Technology. Fredrich is a member of the Editorial Review Committee for SPE Reservoir Evaluation & Engineering.
Greg L. Deitrick is a Senior Research Engineer in Reservoir

Engineering with Shell International Exploration and Production Company in Houston. e-mail: deitrick@shellus.com. He holds a BS degree from the University of Michigan and a PhD degree from the University of Minnesota, both in chemical engineering. **J. Guadalupe Arguello** is a Principal Member of Technical Staff in the Solid Mechanics Engineering Department at Sandia National Laboratories in Albuquerque, New Mexico. e-mail: jgargue@sandia.gov. His interests include advanced computational technology, computational geomechanics, powder mechanics, nonlinear dynamics, solid/structure and fluid/structure interaction. He holds BS, ME and PhD degrees, all in civil engineering from Texas A&M University. **Eric P. de Rouffignac** is a Senior Staff Research Physicist with Shell International Exploration and Production Company in Houston. e-mail: edr@shellus.com. His interests include reservoir engineering, geomechanics, physical properties of materials at high temperature, and measurement of thermal properties of rocks. He holds a BS degree from the National University of Mexico and a PhD degree from the University of Texas at Austin, both in physics.

TABLE 1–OVERBURDEN AND PORCELANITE MATERIAL PROPERTIES (DRUCKER-PRAGER MODEL)

Material	E (psi)	ν	ρ (slugs/ft^3)	α	κ (psi)
Air Sands	18,000	0.30	3.687	0.1733	4.45
Upper and Lower Tulare	35,000	0.25	4.016	0.1398	30.63
Upper Porcelanite	68,000	0.22	3.493	0.1504	122.12
Lower Porcelanite	360,000	0.29	3.784	0.1504	122.12

TABLE 2– DIATOMITE MATERIAL PROPERTIES (CAP PLASTICITY MODEL[18])

Material Parameter	Diatomite G	Diatomite H	Diatomite I	Diatomite J	Diatomite K	Diatomite L	Diatomites M & N
K (psi)	24,090	31,818	32,576.0	33,333	36,161	56,768	82,121
$2G$ (psi)	40,769	53,846	51,923.0	50,000	61,196	96,068	138,974
ρ (slugs/ft^3)	3.008	3.008	3.008	3.008	3.008	3.008	3.008
A (psi)	486.1	407,032.4	135,263.0	394.4	586.6	1,235.0	4,252.2
B (psi^{-1})	7.11E-04	4.24E-07	9.19E-07	1.869E-03	8.61E-04	3.054E-04	1.062E-04
C (psi)	410.4	406,887.9	135,100.0	393.8	444.0	937.5	4,252.0
D_1 (psi^{-1})	0.0	0.0	2.50E-05	5.0E-05	1.0E-05	2.8E-05	2.80E-05
D_2 (psi^{-2})	9.0E-08	9.0E-08	1.30E-07	1.7E-07	0.0	0.0	0.0
R	3.0	4.5	3.03	1.559	1.4	2.5	3.8
W	0.12	0.12	0.165	0.21	0.05	0.08	0.08
X_0 (psi)	0.0	0.0	-100	-200	-183	-183	-183.0

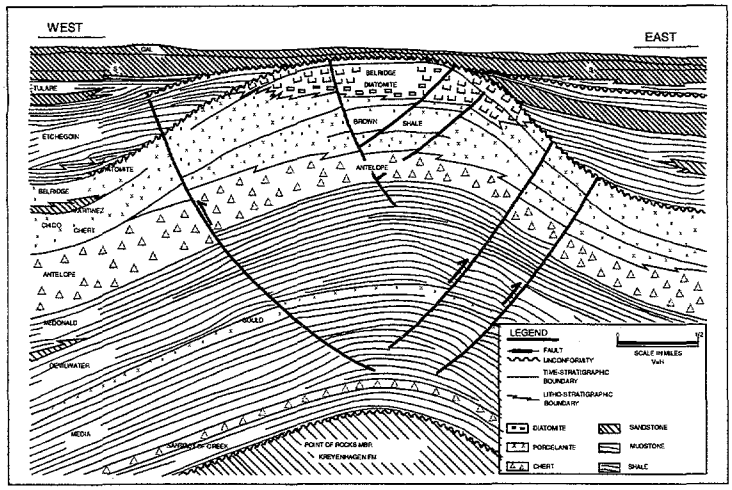

Fig. 1–Geologic east-west cross section of South Belridge Field (Ref 13).

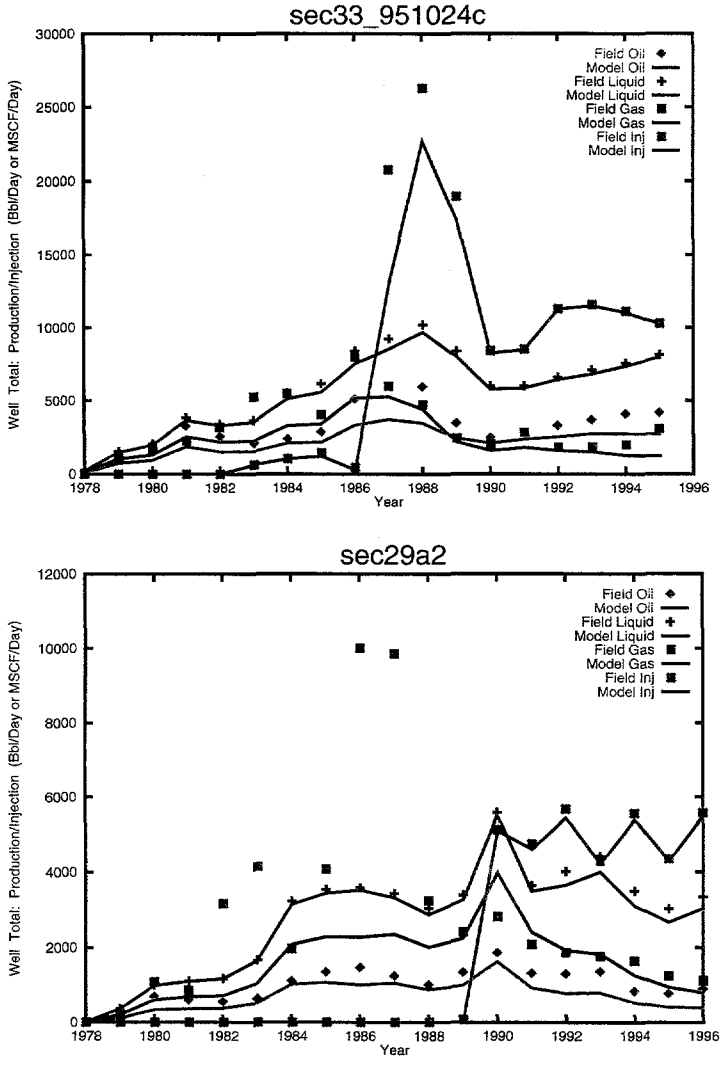

Fig. 2–Comparison of the 3D reservoir simulation for Section 33 (top) and Section 29 (bottom) with the historical field performance. Note that the scale on the *y*-axis is different for the two plots.

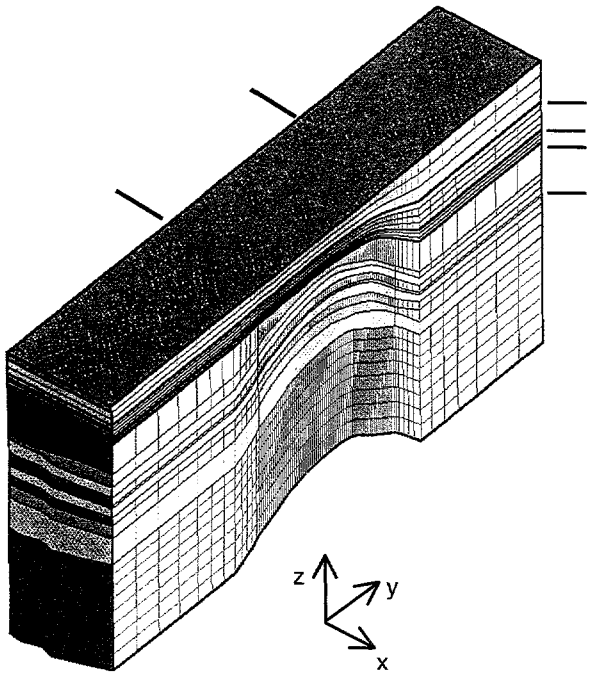

Fig. 3–Finite element geomechanical model of Section 33, South Belridge. The top of the model is at the earth's surface, and the long dimension of the model is oriented N11°E. The locations of the contact surfaces are indicated by the three topmost horizontal lines at the right. The two lower lines mark the top and bottom of the production interval. The areal extent of production is indicated by the two thick lines at the top.

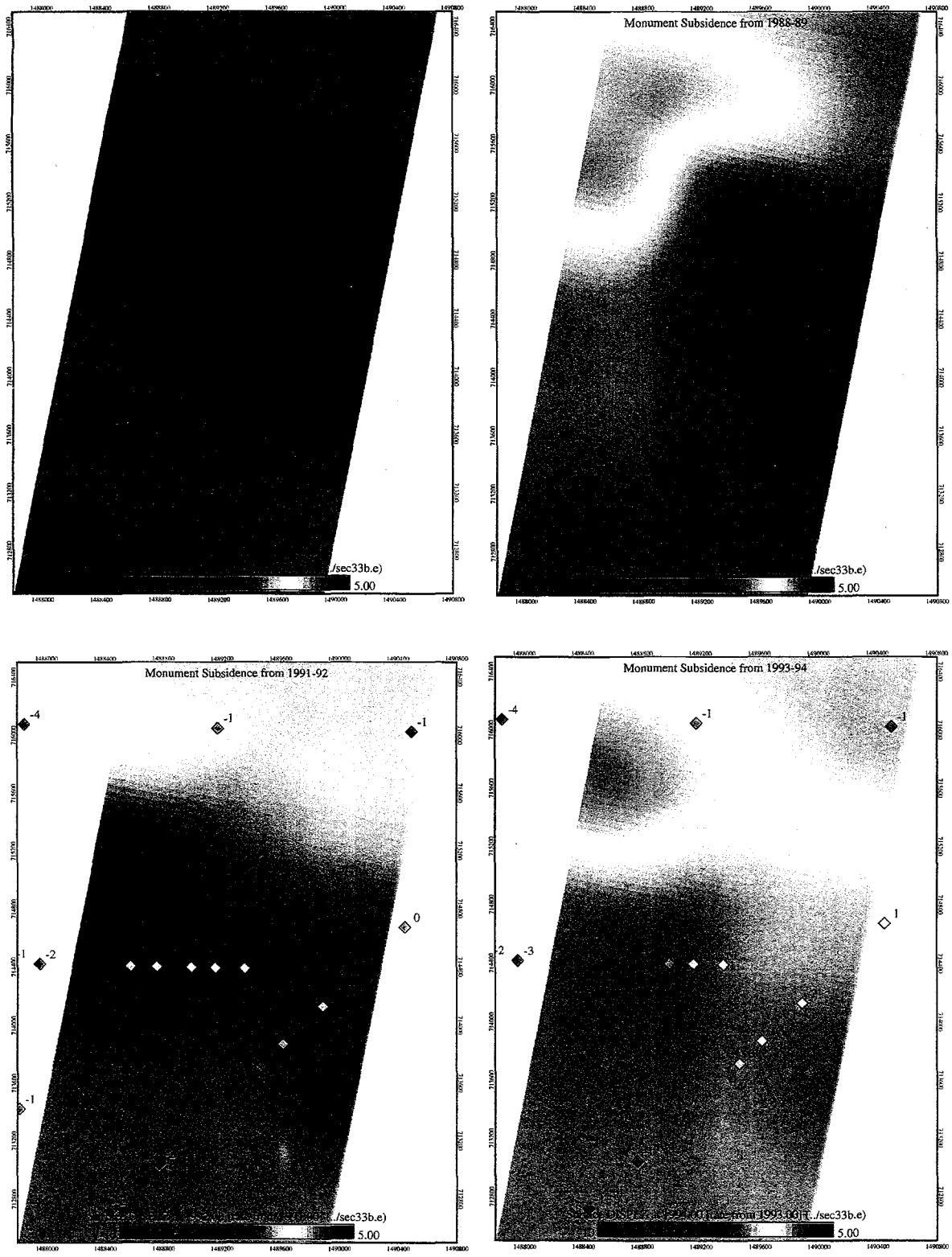

Fig. 4– Map view of subsidence rate at 1987.0 (upper left), 1989.0 (upper right), 1992.0 (lower left), and 1994.0 (lower right) calculated from the prior 1-yr for the Sect. 33 model. The unit for the color scale at the bottom is in/yr, with negative numbers indicating subsidence. The colored diamonds indicate survey monument data for the same time period. Note that only small parts of the flank regions are shown (see Fig. 3).

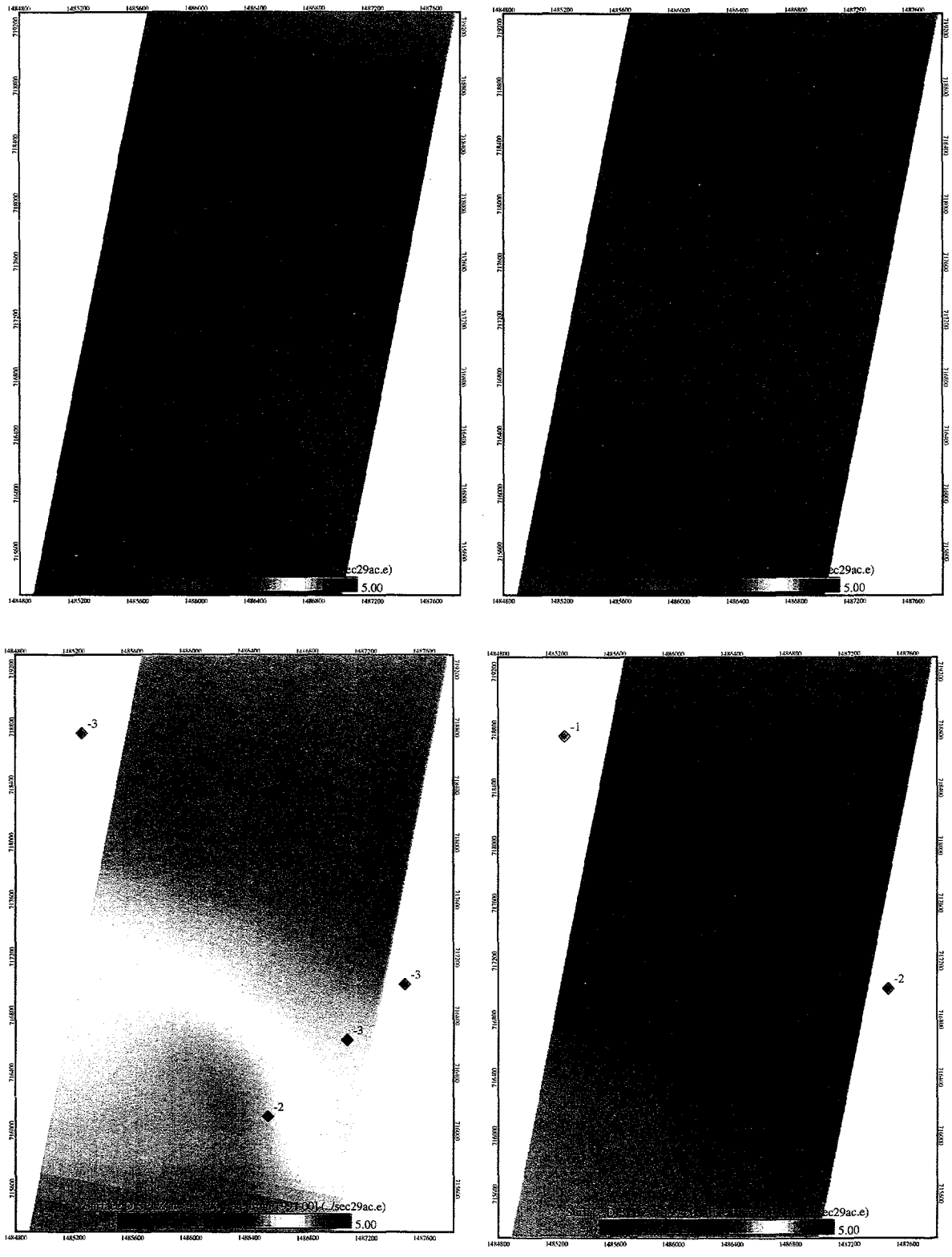

Fig. 5–Map view of subsidence rate at 1987 (upper left), 1989 (upper right), 1992 (lower left), and 1994 (lower right) calculated from the prior 1-yr for the Sect. 29 model. The unit for the color scale at the bottom is in/yr, with negative numbers indicating subsidence. The colored diamonds indicate survey monument data for the same time period. Note that only small parts of the flank regions are shown (see Fig. 3).

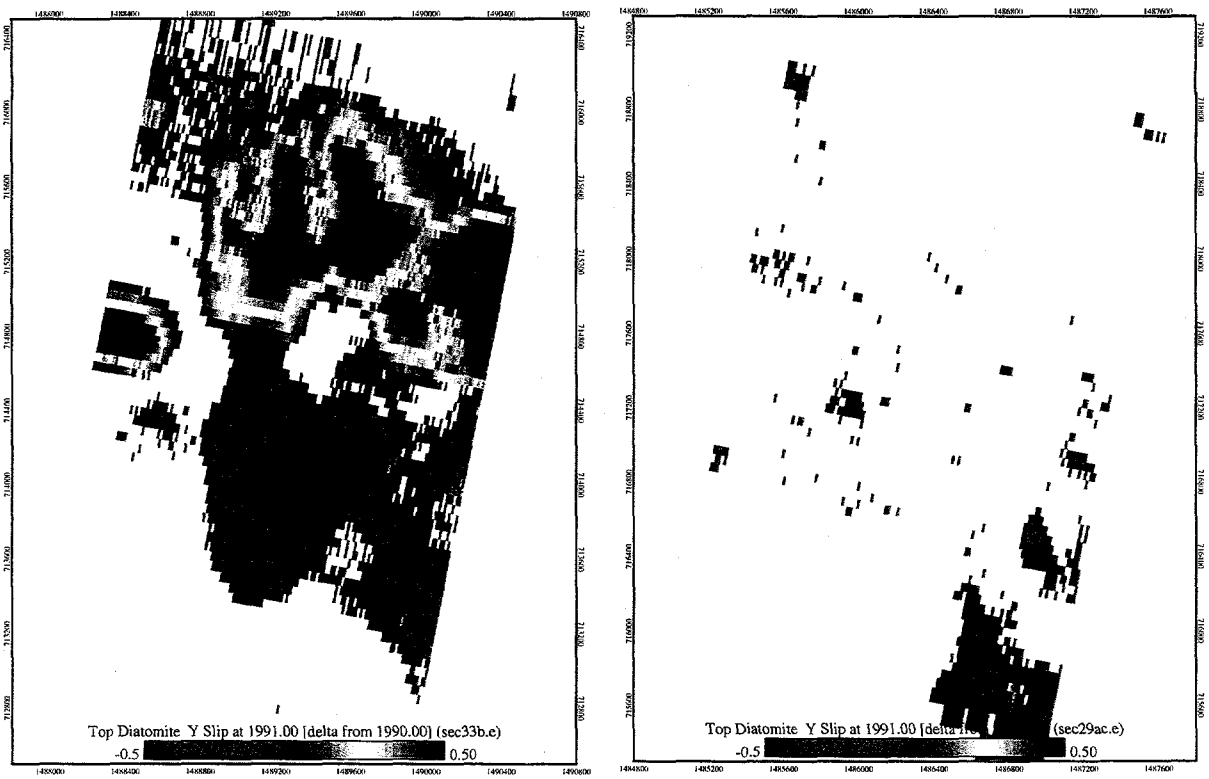

Fig. 6–Map view of predicted incremental horizontal shear displacement in the *y*-direction (parallel to the hydraulic fracture direction) at the top of the diatomite reservoir from 1990-91 (years 12-13 in the simulation). The color scale at the bottom is in in/yr. The Section 33 model (left) indicates shearing displacements of ± ½ foot over large areas. Conversely, the Section 29 model (right) shows very limited shear displacement at the contact surface located immediately above the reservoir. Note that only small parts of the flank regions are shown (see Fig. 3). Also, for clarity, predicted shear displacements of ~0 are not shown.

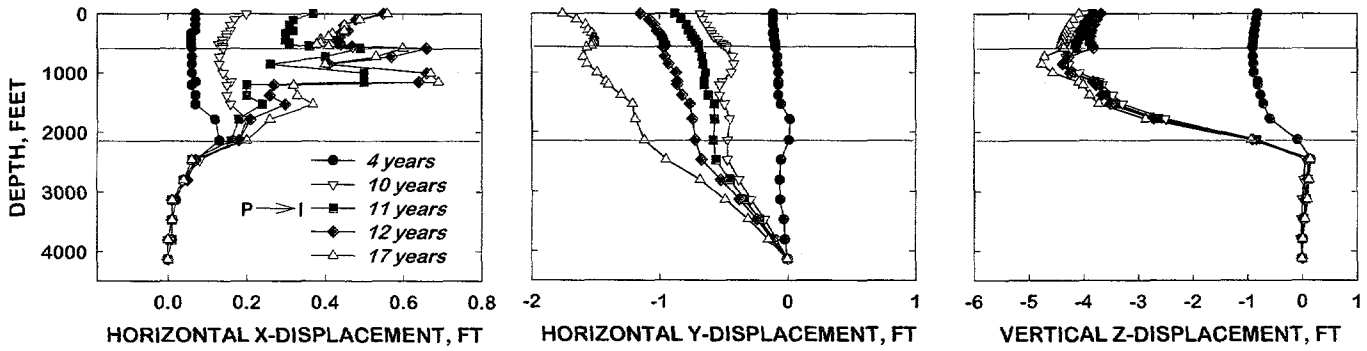

Fig. 7–Nodal displacements at 1982 (year 4.0), 1988 (year 10.0), 1989 (year 11.0), 1990 (year 12.0), and 1995 (year 17.0) as a function of depth in the horizontal *x*-direction (left), horizontal *y*-direction (middle), and vertical *z*-direction (right) at a particular well location for the Section 33 simulation. The horizontal lines bound the reservoir formation, with the upper line a frictional contact surface. Two additional contact surfaces (not indicated) are located further up in the overburden.